

RSC Advances



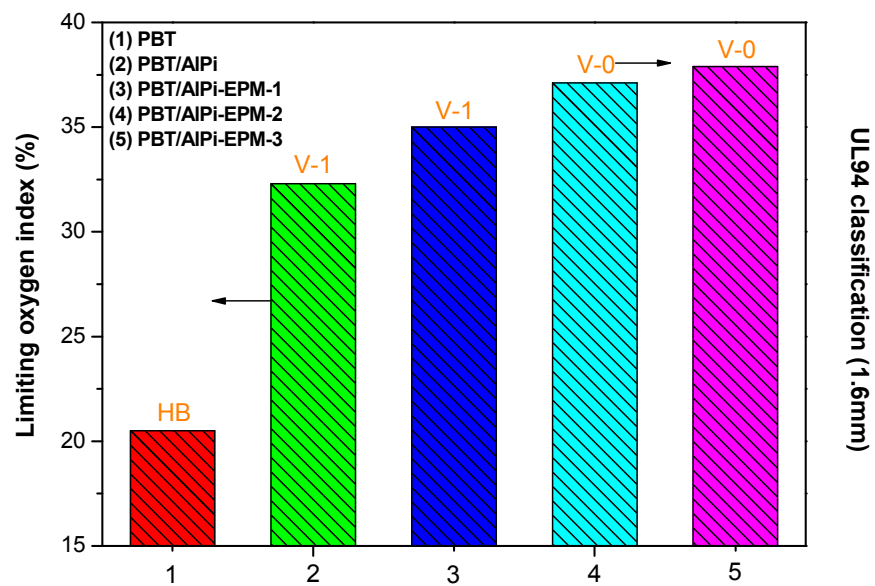
This is an *Accepted Manuscript*, which has been through the Royal Society of Chemistry peer review process and has been accepted for publication.

Accepted Manuscripts are published online shortly after acceptance, before technical editing, formatting and proof reading. Using this free service, authors can make their results available to the community, in citable form, before we publish the edited article. This *Accepted Manuscript* will be replaced by the edited, formatted and paginated article as soon as this is available.

You can find more information about *Accepted Manuscripts* in the [Information for Authors](#).

Please note that technical editing may introduce minor changes to the text and/or graphics, which may alter content. The journal's standard [Terms & Conditions](#) and the [Ethical guidelines](#) still apply. In no event shall the Royal Society of Chemistry be held responsible for any errors or omissions in this *Accepted Manuscript* or any consequences arising from the use of any information it contains.

The manuscript presents an outstanding synergistic effect of aluminum diethylphosphinate (AlPi) and the epoxy-functional polysiloxane (EPM) on preparing flame-retarded PBT.



Cite this: DOI: 10.1039/c0xx00000x

www.rsc.org/advances

PAPER

Flame retardancy mechanism of poly(butylene terephthalate)/aluminum diethylphosphinate composites with an epoxy-functional polysiloxane

Xiao Han,^a Jianqing Zhao,^{a,b} Shumei Liu,^{*a,b} Yanchao Yuan^a

Received (in XXX, XXX) Xth XXXXXXXXX 20XX, Accepted Xth XXXXXXXXX 20XX

DOI: 10.1039/b000000x

The flame retardancy of poly(butylene terephthalate)/aluminum diethylphosphinate (PBT/AIPi) composites was greatly enhanced by the incorporation of an epoxy-functional polysiloxane (EPM). The limiting oxygen index (LOI), vertical burning (UL94) and cone calorimeter test were performed to evaluate the flame-retarded effect. The PBT composite containing 11 wt% AIPi attained a V-0 rating in the UL94 test with LOI of 37.1% by the aid of 0.6 wt% EPM. The flame-retarded mechanism of the PBT/AIPi/EPM composite was also proposed on the results of cone calorimeter test, TGA, TGA-FTIR, SEM micrographs and SEM/EDX analysis of the residues. The introduction of small amounts of EPM encouraged the formation of cross-linking char residue remarkably. The condensed-phase action was proposed to be the dominant flame-retardant role for the PBT/AIPi/EPM composite.

1. Introduction

Poly(butylene terephthalate) (PBT) is widely used in electrical and electronic industry thanks to its good mechanical, thermal, electrical properties and processing advantages. Nevertheless, the high flammability and serious dripping during combustion of neat PBT cannot meet the modern fire safety requirements. The endowment with flame retardancy on PBT is crucial for applications in these fields. Traditional halogenated flame retardants used for thermoplastic polyesters are economic and effective,^{1,2} but their utilizations are restrained due to the release of toxic and corrosive smoke. As one of the major thermoplastic polyesters, the development of halogen-free flame-retarded PBT has become the mainstream nowadays. The most promising routes are founded on the flame retardants containing phosphorus and silicon.³⁻⁵

Phosphorus-based additives such as red phosphorus, inorganic phosphates and organo-phosphorus compounds are the most common halogen-free flame retardants.⁶⁻¹⁰ The attempts have been made to flame-retarded PBT with aryl diphosphates, polyphosphates or 9,10-dihydro-9-oxa-10-phosphaphenanthrene-10-oxide (DOPO) derivatives. 20 wt% triphenyl phosphate (TPP) in combination with 10 wt% melamine helps the neat PBT to attain a UL 94 V-0 rating,⁸ 15 wt% bisphenol A bis(diphenyl phosphate) (BDP) and 15 wt% novolac provide a UL 94 V-0 rating with glass-fiber reinforced PBT;¹¹ The UL 94 V-0 rating of neat PBT is achieved with the addition of 20 wt% DOPO derivative (DOPO-MAH).⁹ Recently, as the novel flame retardants, metal salts of alkylphosphinate and hypophosphorous acid seem to be exceptionally effective in PBT.^{10,12-17} The UL 94 V-0 ratings are fulfilled in glass-fiber filled PBT at the loading of 20 wt% aluminum hypophosphorous acid and aluminum diethylphosphinate (AIPi).^{10,13,16,17} However, under the

circumstances without a synergist, the relatively high loadings (14-20 wt%) of the aforementioned phosphorus-containing flame retardants in PBT and fiber-reinforced PBT will induce adverse effects to the processing feature and mechanical properties of polymer composites.

Silicone derivatives, especially with the branched chain structure and aromatic group, are successfully used as flame retardants in thermoplastic polymers.^{18,19} They can develop a protective silica layer at high temperature and improve the char oxidation resistance, thus the flame retardancy of underlying polymers enhances.²⁰ But none is able to provide sufficient flame retardancy themselves.^{18,19} Recently, the existence of synergistic effect between silicon and phosphorus on flame retardancy has been confirmed.²¹⁻²⁴ Such as 18 wt% zinc phosphinate in combination with 2 wt% octamethyl polyhedral oligomeric silsesquioxane (OMPOSS) increases the LOI value of poly(ethylene terephthalate) (PET) from 26% to 38%,²⁵ but current researches on phosphorus-silicon flame-retarded PBT do not gain satisfactory flame retardancy.

In this work, an epoxy-functional polysiloxane (named as EPM, Fig. 1) was employed for elevating the flame retardancy of PBT/AIPi composites. The loading of AIPi for flame-retarding PBT was reduced by the outstanding synergistic effect of EPM. The flame-retarded mechanism of the obtained PBT/AIPi/EPM composites was investigated.

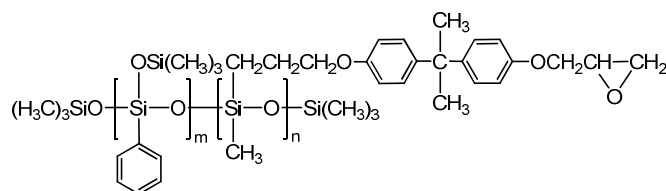


Fig. 1 Schematic chemical structure of EPM.

2. Experimental section

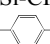
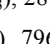
2.1. Materials

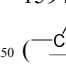
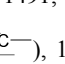
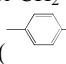
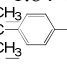
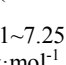
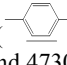
Poly(butylene terephthalate) (PBT, 1100-211M) used in this study was the product of Chang Chun Plastics Co., Ltd, Taiwan.

Aluminum diethylphosphinate (AlPi, Exolit OP 1240) was supplied by Clariant as a commercial product. γ -chloropropylmethyldiethoxysilane (MCPS) and phenyltrimethoxysilane (PTMS) were provided by Tianci Organic Silicon Company (China) and were used as received. EPM was synthesized in our laboratory.

2.2. Preparation of EPM

EPM was prepared by a two-step reaction. Firstly, phenylsilsesquioxane/ γ -chloropropylmethylsiloxane copolymer (PCSi) was synthesized by the hydrolysis copolymerization of γ -chloropropylmethyldiethoxysilane (MCPS) and phenyltrimethoxysilane (PTMS). 0.2 mol MCPS, 0.2 mol PTMS, 100 mL toluene and 4 mL concentrated hydrochloric acid were added into a 500 mL four-necked flask with a mechanical stirrer, a reflux condenser, a thermometer and a dropping funnel. 15 mL distilled water was dropwise added to the reaction mixture, the reaction mixture was stirred and heated to reflux, reacted at 80 °C for 4 h and then at the same temperature for another 4 h with the addition of 0.01 mol end-capping reagent hexamethyldisiloxane (MM). The obtained solution was washed with saturated Na_2SO_4 solution, and separated with a separatory funnel to remove the aqueous phase, then distilled at the reduced pressure to eliminate toluene. Subsequently the product was put in a vacuum oven at 100 °C for 8 h. Liquid PCSi was obtained with a yield of 85.0%.

Then epoxy group was introduced into the side chain of PCSi through the nucleophilic substitution reaction between PCSi, epoxy chloropropane and bisphenol A sodium salt. 0.05 mol bisphenol A, 8 mL 50 wt% NaOH solution and 150 mL absolute alcohol were added into a 250 mL four-necked flask equipped with a mechanical stirrer, a reflux condenser, a thermometer and a nitrogen inlet. Before the reaction, nitrogen was added into the flask to remove oxygen. The reaction was carried out at 80 °C for 1 h with stirring and bisphenol A sodium salt solution (BPA-2Na) was formed. Consecutively, 0.05 mol PCSi was added into the solution and the reaction was kept about 6 h at the same temperature. The reaction mixture was cooled to 50 °C and then reacted for 3 h with the addition of 0.25 mol epoxy chloropropane. After the reaction was over, the solution system was filtered to discard the solid residual, and then distilled under the reduced pressure. Finally, the product was dried at 100 °C under vacuum to constant weight. Liquid EPM was obtained with a yield of 91.2%. The structure and average molecular weight of EPM was characterized by FTIR, $^1\text{H-NMR}$ and GPC. FTIR (KBr) (cm^{-1}): 1030, 1150 (-Si-O-Si-), 1248 (-Si-CH₃), 2874, 2965 (-CH₂), 3053, 1594, 1491, 1431, 697, 740 (—)—, 796, 675 (—)—, 914

(—)—), 1181 (—)—); $^1\text{H NMR}$ (CDCl_3) (ppm): 0.15 (-Si-CH₃), 0.69 (-Si-CH₂-), 1.84 (-Si-CH₂-CH₂-), 3.37 (-Si-CH₂-CH₂-), 1.65 (—)—), 4.17 (—)—), 2.76, 2.90 (—)—), 6.71~7.25 (—)—); The M_n and M_w of EPM were 2270 $\text{g}\cdot\text{mol}^{-1}$ and 4730 with 2.08 of PDI. The accurate content of epoxy groups was 0.154 $\text{mol}\cdot(100\text{g})^{-1}$ determined by hydrogen chloride-acetone titrimetry,²⁶ *ie.* average 3 epoxy

groups per EPM molecule. The results indicate that EPM has been synthesized successfully.

2.3. Specimen preparation

PBT was dried overnight in a vacuum oven at 90 °C before blending. All samples were prepared on a 26 mm LTE26/40 twin-screw extruder (Labtech, Germany) by using an increasing thermal profile, from the hopper to the die section, from 180 to 235 °C and a screw speed of 150 rpm. The obtained pellets were injection molded (injector: EC75N II, TOSHIBA MACHINE Company, Japan) into various shapes, sizes and forms of different test specimens. Five different samples were prepared as shown in Table 1.

2.4. Flammability

The flammability properties of studied samples were determined by using the standard UL 94-2009 vertical tests (specimen size: 120 mm × 12.7 mm × 1.6 mm) on a FTT0082 UL 94 flame chamber (Fire Testing Technology, UK) and by limiting oxygen index (LOI) according to ISO 4589 (specimen size: 150mm × 75 mm × 4 mm) on a FTT0077 oxygen index instrument (Fire Testing Technology, UK).

2.5. Mechanical properties

The tensile strength, flexural strength and modulus were measured using a universal testing machine (Z1010, Zwick, Germany) at the test speed of 50 $\text{mm}\cdot\text{min}^{-1}$ and 20 $\text{mm}\cdot\text{min}^{-1}$ according to ISO 527:1996 and ISO 178:2003 respectively. The Izod notched impact strength were determined by a pendulum impact tester (5113, Zwick, Germany) according to ISO 180:2001. Five specimens were tested for each sample in both measurements to obtain a reliable average value and standard deviations.

2.6. Pyrolysis

Thermogravimetric analysis (TGA) was performed using a STA449C (Netzsch, Germany) with a nitrogen flow of 30 $\text{mL}\cdot\text{min}^{-1}$ at a heating rate of 20 $^\circ\text{C}\cdot\text{min}^{-1}$ from the room temperature to 700 °C. The sample weight was about 10 mg. TGA was coupled with a Tensor 27 FTIR spectrometer (Bruker, Germany) for TGA-FTIR investigation. The transfer tube with an inner diameter of 1mm was heated to 230 °C and the analysis cell to 230 °C. Product release rates were evaluated using the height of product-specific peaks as a function of time.

2.7. Fire behavior

A FTT0007 cone calorimeter (Fire Testing Technology, UK) was used to characterize the forced-flaming behavior, according to ISO 5660. Each specimen (100 mm × 100 mm × 6 mm) was wrapped in an aluminum foil and exposed horizontally to 35 $\text{kW}\cdot\text{m}^{-2}$ external heat flux. A retainer frame was also used to reduce unrepresentative edge-burning. The decreased sample area was taken into account for the calculation. The flame-out was defined as the end of test.

2.8. Residue analysis

The residues collected after TGA-FTIR and cone calorimeter measurement were analyzed by means of FTIR spectroscopy on a Vertex 70 FTIR spectrometer (Bruker, Germany). The residue

analysis was performed using scanning electron microscopy, SEM (FEI Quanta 200, Netherlands), and energy dispersive X-ray spectroscopy, EDX (Oxford Inca Energy350, UK).

3. Results and discussion

3.1. Flammability and mechanical properties

Table 1 The flammability and mechanical properties of PBT, PBT/AlPi and PBT/AlPi/EPM composites

Samples	Formulation (wt%)			LOI (%)	UL94, 1.6 mm bar			Tensile strength (MPa)	Flexural strength (MPa)	Flexural modulus (GPa)	Izod notched impact strength (J·m ⁻¹)
	PBT	AlPi	EPM		t ₁ /t ₂ ^a	dripping	rating				
	PBT	100	/		/	20.5	BC ^b				
PBT/AlPi	88	12	/	32.3	5.3/7.9	yes	V-1	44.0±0.7	83.2±0.4	2.92±0.08	39.7±0.8
PBT/AlPi/EPM-1	88.6	11	0.4	35.0	6.5/4.6	no	V-1	54.0±0.7	91.7±0.5	2.99±0.12	47.4±0.7
PBT/AlPi/EPM-2	88.4	11	0.6	37.1	1.7/2.1	no	V-0	54.3±0.6	92.3±0.4	3.15±0.15	48.5±0.5
PBT/AlPi/EPM-3	88	11	1.0	37.9	2.0/2.2	no	V-0	54.7±0.2	93.2±0.5	3.17±0.20	49.1±0.4

^at₁ and t₂ (s), average combustion times after the first and the second applications of the flame;

^bBC, burns to clamp.

The UL 94 and LOI tests were performed to investigate the fire performance of PBT, PBT/AlPi and PBT/AlPi/EPM composites. The results are illustrated in Table 1. PBT was a highly flammable material with LOI of 20.5%. The addition of AlPi into PBT resulted in a moderate improvement in LOI by reaching 32.3%. The composites including both AlPi and EPM showed a steady increase in LOI by reaching 37.9% in PBT/AlPi/EPM-3. PBT could not extinguish itself, and there was a serious flaming dripping. Hence it only achieved HB classification in terms of UL 94. In presence of 12 wt% AlPi, PBT/AlPi composite received a V-1 classification and the dripping phenomenon was also observed. The good results in UL 94 (V-0 rating) were accomplished with the combination of 11 wt% AlPi and 0.6 or 1.0 wt% EPM. The dripping was totally suppressed. Although the correlation of LOI and UL 94 is not self-evident,²⁷ the results of LOI and UL 94 are consistent with each other undoubtedly in this work. With the addition of EPM, the flame retardancy of PBT/AlPi was strengthened even further. According to the above results, a synergistic effect between AlPi and EPM is proposed

for PBT.

The tensile strength, Izod notched impact strength, flexural strength and modulus of PBT, PBT/AlPi and PBT/AlPi/EPM composites were also listed in Table 1. The incorporation of AlPi in PBT induced a perceptible reduction in mechanical properties, maybe attributed to the degradation of PBT caused by AlPi¹² and the stress concentration effect of AlPi particle agglomerate.¹³ However, a positive trend in the mechanical performance of PBT/AlPi/EPM composites was observed. The tensile strength, flexural strength, flexural modulus and Izod notched impact strength of PBT/AlPi/EPM composites enhanced with increasing EPM content. Noteworthy, the tensile and flexural strength were even higher than those of neat PBT. This phenomenon implied the occurrence of chain extension and cross-linking effect caused by EPM in extrusion process. Due to its sufficient flame retardancy and good mechanical properties, PBT/AlPi/EPM-2 was taken as the representative of PBT/AlPi/EPM composites discussed in the following part.

3.2. Thermal degradation behavior

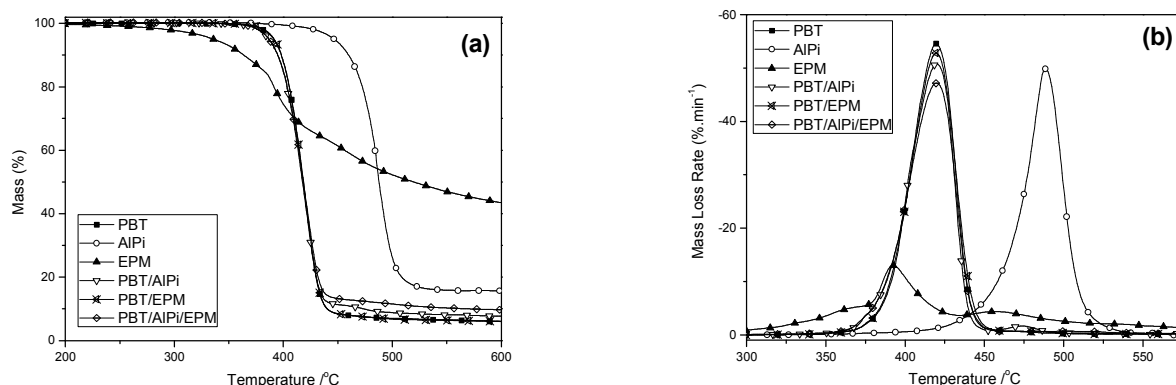


Fig. 2 (a) TG and (b) DTG curves of PBT, AlPi, EPM, PBT/AlPi, PBT/EPM and PBT/AlPi/EPM-2 in N₂ at 20 °C·min⁻¹.

The distinct difference in LOI and UL 94 rating among PBT, PBT/AlPi and PBT/AlPi/EPM could be ascribed to the variation in their flame retardancy mechanism. The results of TGA investigation of all kinds of materials are summarized in Fig. 2 and Table 2. An one-step degradation was observed for PBT from 355 °C to 449 °C, with the T_{max} at 419 °C and only 4.8 wt% solid residue at 700 °C.

Addition of AlPi, EPM or both AlPi and EPM did not fundamentally change the main degradation process of PBT. The onset degradation temperature (indicated by $T_{5\%}$) and the main mass loss of PBT/AlPi, PBT/EPM and PBT/AlPi/EPM-2 composites were slightly changed compared to PBT, while their T_{max1} in the first mass loss step was almost the same around 420 °C. In comparison with PBT, the addition of 12 wt% AlPi caused an increase of 2.8 wt% in the residue which might correspond to the inorganic aluminum phosphates from AlPi degradation and additional carbonaceous char.¹² In addition, the sample of PBT/AlPi showed an additional minor degradation step with 3.8 wt% mass loss from 452 °C to 495 °C.

Simultaneously, the addition of 0.6 wt% of EPM in PBT and PBT/AlPi composite caused a raise of approximate 1 wt% and 2 wt% residue at 700 °C separately, clearly more than expected from the residue by the degradation of EPM itself. Moreover, the additional small degradation step from 452 °C to 495 °C for PBT/AlPi composite had vanished. According to the analysis mentioned above, it may prove that some extra interactions exist among PBT, AlPi and EPM during the degradation process.

Table 2 TGA data of all samples (20 °C·min⁻¹)

Samples	$T_{5\%}$ (°C)	1st stage		2nd stage		Residue at 700°C (wt%)
		Mass Loss (wt%)	T_{max1} (°C)	Mass Loss (wt%)	T_{max2} (°C)	
PBT	390	94.0	419	/	/	4.8
AlPi	447	84.4	489	/	/	15.5
EPM	336	35.4	392	21.4	457	40.4
PBT/AlPi	386	88.7	420	3.8	474	7.6
PBT/EPM ^a	391	92.9	421	/	/	5.7
PBT/AlPi/EPM-2	387	90.4	420	/	/	9.4

^aPBT/EPM=99.4/0.6 (wt%).

3.3. Evolved gas analysis

The main evolved degradation products of PBT include butadiene, carbon dioxide (CO₂), tetrahydrofuran (THF), benzoic acid and terephthalic esters according to the literature.²⁸ Some complex aromatic species also volatilize at the end of degradation stage. It should be noted that terephthalic acid cannot be detected in the gas phase, condensing in the transfer line and the outlet of the thermogravimetric due to its high sublimation point.

Fig. 3 shows the FTIR spectra of the evolved gas of PBT/AlPi and PBT/AlPi/EPM-2 at the same T_{max1} =420 °C (for

both PBT/AlPi and PBT/AlPi/EPM-2 corresponded to the spectrum at the heating time of 1149 s) from TGA-FTIR analysis. The gaseous products of PBT/AlPi (Fig. 3a) are consistent with the literature.^{14,29} Diethylphosphinic acid (3649, 856 and 770 cm⁻¹) was the characteristic degradation product of AlPi. Also butadiene (908 cm⁻¹), CO₂ (2358 cm⁻¹), THF (2978 cm⁻¹), benzoic acid (3584 and 1764 cm⁻¹) and terephthalic esters (1745 and 1267 cm⁻¹) were detected. During the additional degradation step, ethene (950 cm⁻¹), benzene (672 cm⁻¹) and CO₂ were identified according to their characteristic signals and the disproportionate ratio between the signal intensity at 669 cm⁻¹ and 2358 cm⁻¹.¹⁷ THF, CO₂, diethylphosphinic acid and butadiene were also released during the degradation process of PBT/AlPi/EPM-2 (Fig. 3b). Obviously, the addition of EPM induces a great discrepancy on the evolved gas spectrum and the absorption band intensity distinctly diminishes compared to PBT/AlPi. As the model degradation derivatives of PBT, the characteristic absorption bands of benzoic acid (3584 and 1764 cm⁻¹) and esters (1745 and 1267 cm⁻¹) can hardly be found. Furthermore, the signal of diethylphosphinic acid (3649, 856 and 770 cm⁻¹) was also clearly weakened. No silicon compound signals were detected.

The product release rates of all materials are presented in Fig. 4. The CO₂ release rate (Fig. 4a) of PBT showed one maximum at 1160s, related to the main mass loss step at 419 °C. In comparison to PBT, the CO₂ release rates for PBT/AlPi and PBT/AlPi/EPM-2 were generally reduced. Moreover, the CO₂ release peak position showed somewhat earlier than in PBT. PBT/AlPi exhibited two maxima in the CO₂ release rate. The first peak was ascribed to the major mass loss step at 1140s (417 °C), and the second peak corresponded to the additional degradation step at about 1320s (483 °C), probably related to the degradation of aluminum phosphinate-terephthalate intermediate.^{15,29} With the combination of EPM in PBT/AlPi, an apparent shift was observed that only one peak in CO₂ release rate existed at 1142s (417 °C) with the reduction in its peak value.

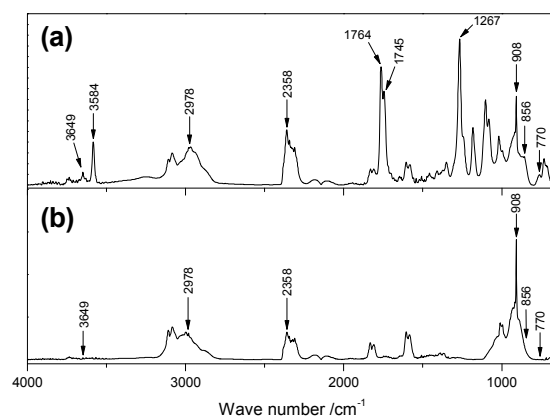


Fig. 3 FTIR spectra of the evolved gases for (a) PBT/AlPi and (b) PBT/AlPi/EPM-2 at 1149s (420 °C).

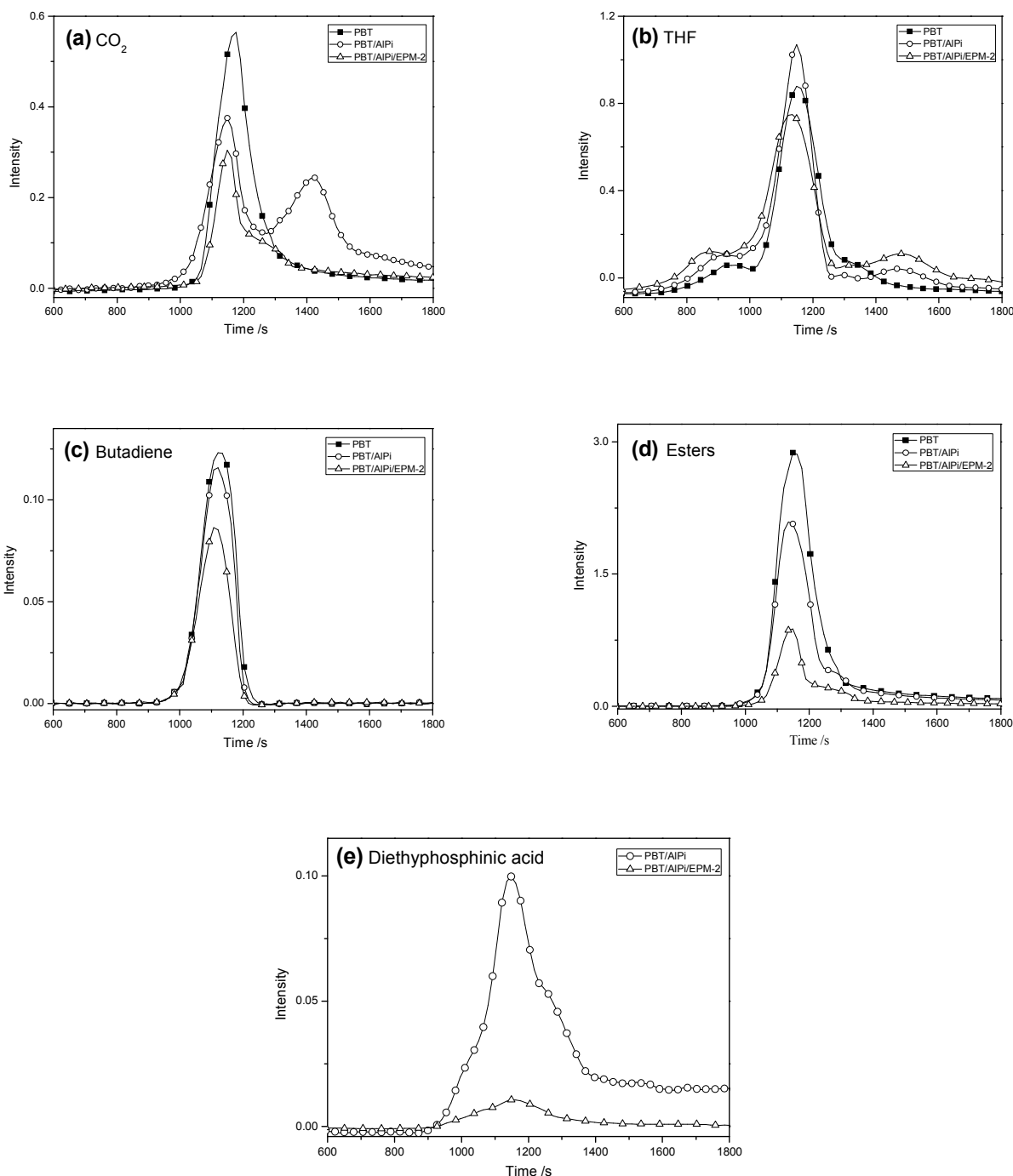


Fig. 4 The product release rates of PBT, PBT/AIPi and PBT/AIPi/EPM-2 determined by TGA-FTIR: (a) CO_2 , (b) THF, (c) butadiene, (d) esters, (e) diethylphosphinic acid.

The THF release rates of PBT, PBT/AIPi and PBT/AIPi/EPM-2 in Fig. 4b evidenced a large difference. PBT exhibited one maximum release rate around 1146s (414 °C). It is worthwhile noting that the shapes of the release rate curve in PBT/AIPi and PBT/AIPi/EPM-2 have changed. For PBT/AIPi, the product release rate increased slightly and a new minor peak around 1480s (506 °C) appeared compared with that of PBT, whereas in PBT/AIPi/EPM-2, the first peak (1119s) related to the

major degradation process (420 °C) decreased compared to PBT; accompanied by the clear enhancement of the second peak (1480s) in contrast to PBT/AIPi. A change was proposed in the PBT ester scission pathway²⁸ according to the difference in THF release rates between PBT/AIPi and PBT/AIPi/EPM-2, and more ester intermediates containing phosphorus and silicon element may be formed for PBT/AIPi/EPM-2 during heating, thus the degradation process of PBT is prolonged.

Although the patterns of release rate curves for butadiene and esters of PBT/AlPi and PBT/AlPi/EPM-2 (Fig. 4c and 4d) did not change, the distinct difference in peak values was revealed in comparison with PBT. For PBT/AlPi, a moderate decrease was obtained. With the further combination of EPM in PBT/AlPi, the release rate intensities of butadiene and esters exhibited a more evident reduction than those for PBT, suggesting an obvious variation in the degradation pathway of PBT.

The release of diethylphosphinic acid (Fig. 4e) in the gas phase diminished spectacularly in PBT/AlPi/EPM-2 composite in contrast to PBT/AlPi. It proves that the combination of EPM could affect the competitive process of phosphorus on whether to volatilize into the gas phase or to retain in the condensed phase, more phosphorus may contribute to the subsequent formation of residue.

The results of evolved gas analysis indicated that the presence of EPM changed the gas release behavior of PBT, resulting in the variation of degradation pathway of PBT. As a reactive polysiloxane containing multi-epoxy group, EPM may react with the degradation products of PBT and AlPi simultaneously, such as benzoic acid, ester derivatives or phosphinic acid. In addition, no silicon signal was monitored in the evolved gas, the silicon group in EPM may not act in gas phase.

3.4. FTIR analysis of the residue

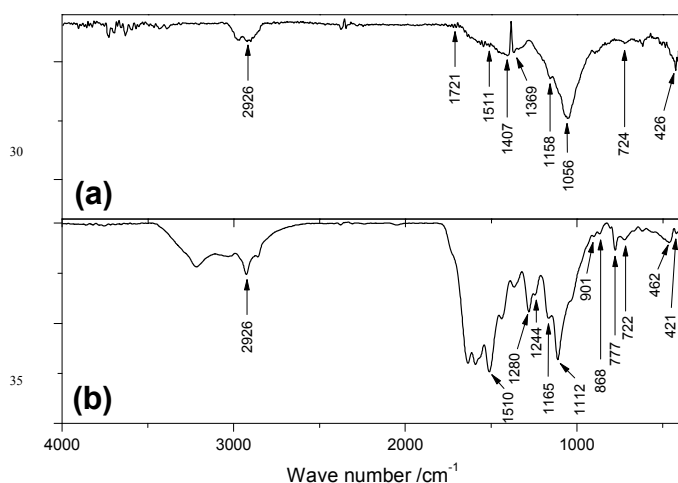


Fig. 5 FTIR spectra of (a) PBT/AlPi and (b) PBT/AlPi/EPM-2 residues.

The residues of PBT/AlPi and PBT/AlPi/EPM-2 obtained after TGA-FTIR measurement were investigated by FTIR to reveal the degradation reactions. In presence of AlPi (Fig. 5a), the peaks of the aromatic group (1511 cm^{-1} , 1407 cm^{-1} and 724 cm^{-1}), anhydride group (1721 cm^{-1} and 1158 cm^{-1}) and aluminum phosphates (1369 cm^{-1} , 1056 cm^{-1} and 426 cm^{-1}) were observed. It is noteworthy that the spectrum of PBT/AlPi/EPM-2 has changed distinctly (Fig. 5b). The hydrocarbon structure is identified by the bands at 2926 cm^{-1} and 1400~1500 cm^{-1} . The strengthened absorption bands at 1510 cm^{-1} , 777 cm^{-1} and 722

cm^{-1} ascribed to the polyaromatic structure indicate that a pronounced aromatization during degradation is invoked. A series of strong absorption bands among 1400 cm^{-1} and 1600 cm^{-1} indicate the appearance of cross-linking carbon-oxygen structure.³⁰ The signals at 1280 cm^{-1} , 1165 cm^{-1} , 901 cm^{-1} , 868 cm^{-1} , 462 cm^{-1} and 421 cm^{-1} belonging to P=O, P-O-C, P-O-P, P-O, O-P-O and O=P-O groups respectively³¹ confirm the presence of various polyphosphates. Moreover the absorption peaks at 1112 cm^{-1} and 1244 cm^{-1} attributed to Si-O-C and Si-C were observed. All the bands in PBT/AlPi/EPM-2 residue confirm the occurrence of cross-linking char containing phosphorus and silicon.

3.5. Possible degradation pathway

According to the established thermal degradation process of PBT,^{1,29} an intramolecular six-member cyclic transition state results in the release of butadiene, CO_2 , THF, terephthalic acid and ester derivatives, and no significant solid residue accompanies. A model for the degradation of PBT and PBT/AlPi has been proposed (Fig. 6a and 6b) according to the literature^{14,15,29} and the above results. AlPi decomposes mainly through the formation of diethylphosphinic acid in the gas phase, which induces the main degradation pathway of PBT to change. The interaction between phosphinate anions and terephthalic acid leads to the formation of Al-phosphinate terephthalate salts during the major degradation stage, which decomposes further in the second minor degradation step around 470 $^{\circ}\text{C}$. Benzene, CO_2 and ethene are released based on the cleavage of the P-ethyl group and the decarboxylation of the terephthalic anion, while various aluminum phosphate derivatives (aluminum orthophosphate, aluminum pyrophosphate and aluminum polyphosphate) are left in the condensed phase.

When both AlPi and EPM are added, the degradation course of PBT varies apparently. According to considered interactions between PBT, AlPi and EPM, the possible degradation models are illustrated in Fig. 6c. As a silicone containing reactive epoxy groups in the branched chain and methyl/phenyl structure in the main chain, EPM acts as both stabilizer and cross-linking agent for the degradation products of PBT and AlPi during combustion.^{18,32,33} Naturally, EPM prefers to react with the carboxylic acid-terminated degradation products, such as terephthalic acid and its derivative Al-phosphinate terephthalate.¹⁹ This interaction results in the lower concentration of esters which are emitted to the gas phase. As a consequence, the release rate of esters will decrease remarkably and the second small peak of CO_2 release vanishes. Furthermore, more phosphorus retains as char in the condensed phase and only a little phosphorus is released into the gas phase as diethylphosphinic acid. The above-mentioned deduction accords remarkably with the TGA-FTIR gas phase measurement and FTIR analysis of the residue. With the raise of temperature, a cross-linking residue containing different kinds of phosphate, siloxane structure and condensed polyaromatic structure has been formed eventually.

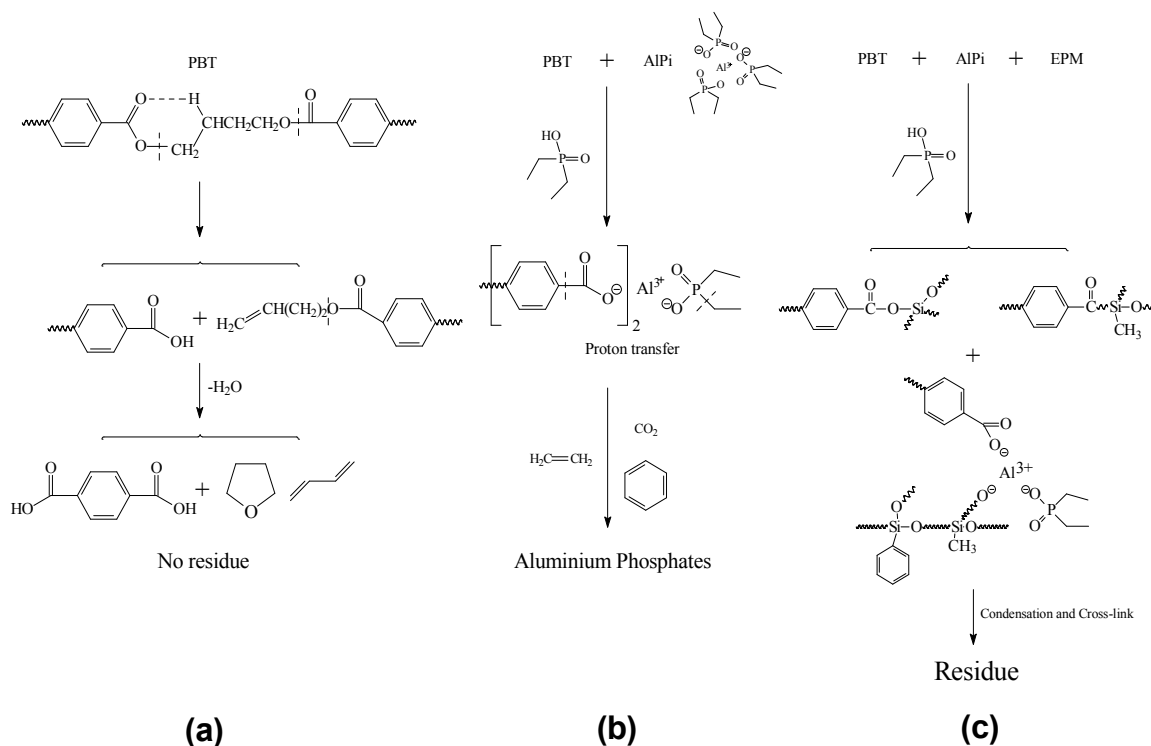


Fig. 6 Possible degradation pathway of (a) PBT, (b) PBT/AIPi and (c) PBT/AIPi/EPM.

3.6. Fire behavior under forced-flaming condition

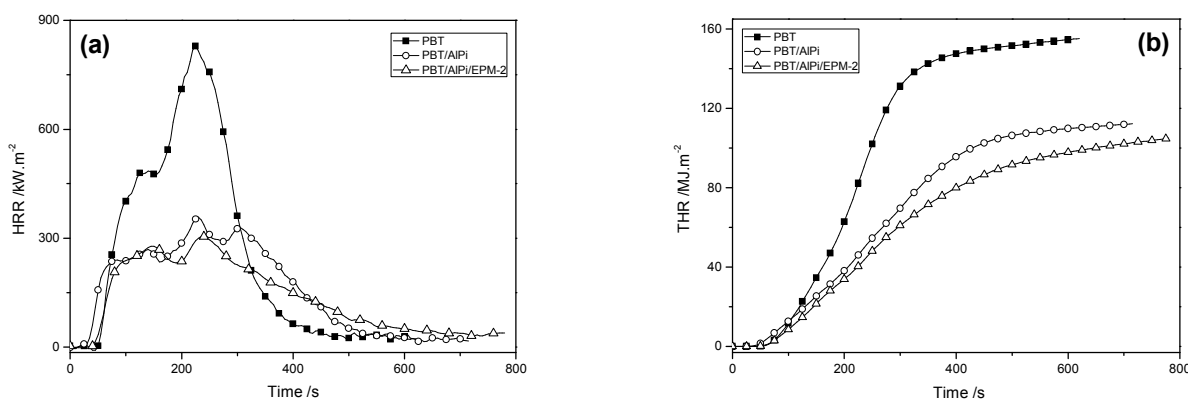


Fig. 7 (a) HRR and (b) THR curves of PBT, PBT/AIPi and PBT/AIPi/EPM-2 at 35 kW·m⁻².

Table 3 CONE calorimeter results for PBT, PBT/AIPi and PBT/AIPi/EPM-2 (irradiance 35 kW·m⁻²)

Samples	t_{ign} (s)	pHRR (kW·m ⁻²)	THE (MJ·m ⁻²)	EHC (MJ·m ⁻² ·g ⁻¹)	pRSR (m ² ·s ⁻¹ ·m ⁻²)	TSR (m ² ·m ⁻²)	Residue (wt%)
PBT	34	839	155	2.1	19.6	3377	2.8
PBT/AIPi	24	365	113	1.4	24.7	5701	7.2
PBT/AIPi/EPM-2	31	312	105	1.7	20.7	3814	11.4

The fire behavior and flame retardancy mechanism of PBT, PBT/AIPi and PBT/AIPi/EPM-2 were demonstrated through the

measurement of cone calorimeter. The data collected from cone calorimeter investigation includes the time to ignition (t_{ign}), heat release rate (HRR), peak value of heat release rate (pHRR), total heat release (THR), effective heat of combustion (EHC), total smoke release (TSR), peak value of the rate of smoke release (pRSR) and residue. The results are summarized in Table 3.

The t_{ign} of PBT was 34 s, and decreased significantly to 24 s with the introduction of AlPi alone. But the t_{ign} for PBT/AlPi/EPM-2 was 31 s, only slightly diminished (ca.3s) compared to neat PBT. The facts imply that AlPi prompts the earlier degradation of PBT while EPM provokes the cross-linking char formation and stabilization for PBT which correspond to the results of pyrolysis behavior analysis mentioned above.

Fig. 7 shows the HRR and THR curves. The HRR curve for PBT was characterized by a large sharp peak with a pHRR value of $839 \text{ kW}\cdot\text{m}^{-2}$. The HRR curve of PBT/AlPi showed a notable reduction and the pHRR was reduced by about 56%, a prolonged burning time occurred in comparison to PBT. A plausible explanation for these facts may lie in the formation of non-stable intermediary char barrier.^{17,29} Al-phosphinate terephthalate attributed as a protective char barrier was formed after ignition, but it decomposed with the elevation of temperature. The pattern of the HRR curve for PBT/AlPi/EPM-2 deviates from PBT and PBT/AlPi, a broad steady plateau presented after an initial increase, simultaneously with an even longer burning time. A positive interaction was fulfilled in PBT/AlPi/EPM-2, the further reduction in the HRR value and pHRR (around 15%) was achieved compared to PBT/AlPi. The total heat evolved (THE=total heat release at flame-out) showed a dramatic reduction from $155 \text{ MJ}\cdot\text{m}^{-2}$ of PBT to $113 \text{ MJ}\cdot\text{m}^{-2}$ of PBT/AlPi and $105 \text{ MJ}\cdot\text{m}^{-2}$ of PBT/AlPi/EPM-2. The THE represents the fire loading of the materials, and depends on the total amount of fuel released and the efficiency of the combustion of volatiles. If there exist char forming and flame inhibition, less flammable volatile degradation products would be emitted and the combustion efficiency on fire should decrease. Consequently, THE will diminish clearly. The HRR and THR curves are associated with the char-forming action,³⁴ where EPM is capable of provoking cross-linking char formation and strengthens the barrier effect. It is believed that a cross-linking residue containing silicon has an enhanced oxidation resistance,^{18,33} and will maintain until the end of combustion. In comparison with PBT/AlPi, PBT/AlPi/EPM-2 demonstrates an apparent reduction in the pHRR and THE, suggesting the occurrence of a synergism among PBT, AlPi and EPM.

The EHC represents the total heat evolved per total mass loss on combustion for the analysis of the flame retardancy mechanism in gas phase during the forced-flaming combustion. A reduction in this item reflects the action of flame inhibition or fuel dilution,³⁴ while flame inhibition usually causes evident decrease in the EHC value. Compared with PBT, a legible reduction of around 33% in the EHC ($1.4 \text{ MJ}\cdot\text{m}^{-2}\cdot\text{g}^{-1}$) for PBT/AlPi was ascribed to the gaseous flame inhibition product of diethylphosphinic acid from AlPi. This flame inhibition effect is well correlated with the THE results. In PBT/AlPi/EPM-2, the EHC value moderately increased from 1.4 to $1.7 \text{ MJ}\cdot\text{m}^{-2}\cdot\text{g}^{-1}$,

accompanied by the declination of the flame inhibition effect. As clarified by the evolved gas analysis, this phenomenon is ascribed to the reduction in the release of diethylphosphinic acid. When the interaction among terephthalate derivatives, phosphinate anions and EPM occurs, less phosphorus will be released to the gas phase but more contributes to the formation of residue.

The smoke release, resulting from the products of incomplete oxidation, is not only used to evaluate the fire hazards, but also reflects the gas phase flame retardancy action. An obvious increase in smoke release usually indicates the existence of flame inhibition effect because of suppression in the oxidation process. The large increase in the pRSR and TSR of PBT/AlPi, about 26% and 69% more than those of neat PBT respectively, supports the conclusion drawn from the results of the EHC that AlPi in PBT mainly acted through radical trapping effect in the gas phase. Nevertheless, the pRSR and TSR of PBT/AlPi/EPM-2 were sharply reduced compared to PBT/AlPi. The TSR was diminished around 33% to $3814 \text{ m}^2\cdot\text{m}^{-2}$ and the pRSR was also decreased about 16% to $20.7 \text{ m}^2\cdot\text{s}^{-1}\cdot\text{m}^{-2}$. The interpretation is consistent with the analysis of the EHC that more phosphorus was kept as inorganic phosphates in the condensed phase as less phosphorus was emitted into the gas phase.

The residues of PBT/AlPi and PBT/AlPi/EPM-2 were generally increased at the end of test in contrast to PBT. For PBT/AlPi, residue of 7.2 wt% was obtained. Concluded from the mass loss results and degradation model, a small amount of EPM combined with PBT/AlPi can cause an evident increase in carbonaceous char, which indicates a predominant condensed phase mechanism in the PBT/AlPi/EPM-2, accompanied by the residue of 11.4 wt%. This unusual increase in the residue of PBT/AlPi/EPM-2 cannot be simply ascribed to the superposition of the residues from the degradation of PBT, AlPi and EPM respectively. Naturally, the results from cone calorimeter investigation defend the conclusion by the existence of flame-retarded synergism in PBT/AlPi/EPM composite. The flame inhibition effect in PBT/AlPi/EPM becomes the minor flame retardancy action.

3.7. SEM/EDX analysis of the residue

To further study the flame retardancy mechanism of PBT, PBT/AlPi and PBT/AlPi/EPM composite, the residue from cone calorimeter measurement was analyzed by means of SEM. The morphologies of the surface of the residual char layer for PBT, PBT/AlPi and PBT/AlPi/EPM-2 are illustrated in Fig. 8. For PBT, the char was loose and fragile, resulting in the poor barrier effect. The addition of AlPi in PBT caused a clear shift in the structure of residue. A bubble-like and porous char was observed maybe due to the impact of plenty of gaseous products. This phenomenon supports that AlPi mainly acts in the gas phase by the release of diethylphosphinic acid.^{15,17,29} The SEM photograph of PBT/AlPi/EPM-2 residue illustrated a smooth, continuous and solid char layer surface, which provides a better protection for the underlying matrix from the thermal-oxidative degradation. As a result, an excellent barrier action for the residue of PBT/AlPi/EPM-2 occurs.

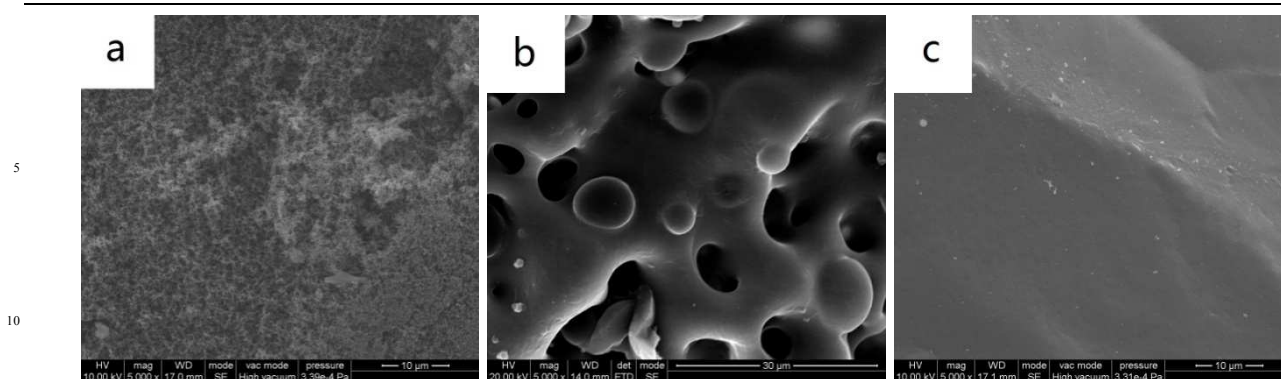


Fig. 8 SEM morphologies of char residue after cone tests: (a) PBT, (b) PBT/AlPi, (c) PBT/AlPi/EPM-2.

The element components of the residue were analyzed through EDX measurement and the results are listed in Table 4. For PBT/AlPi, the residue consisted of relatively high content of carbon, oxygen, phosphorus and aluminum in comparison with its original sample, indicating the existence of some condensed phase actions besides the major flame inhibition behavior in gas phase. The various aluminum phosphates and carbonaceous char were formed. Remarkably, apart from the accumulation of silicon on the surface of the residue, an even higher content of aluminum

and phosphorus was presented in PBT/AlPi/EPM-2, leading to the improvement in the stability and barrier effect of char. Furthermore, the oxidation resistance property of the residue was improved by the enrichment of silicon.^{19,33} The presence of EPM prompted the formation of cross-linking residual char containing aluminum phosphates, siloxane structure and condensed polyaromatic structure. The residue will effectively suppress the transport of heat and fuel, naturally weakens the flame and smoke.

Table 4 The element component of PBT, PBT/AlPi and PBT/AlPi/EPM-2 measured by SEM/EDX

		Element component (wt%)				
		C	O	Al	P	Si
PBT	Original	65.45	29.09	/	/	/
	Residue	63.50	36.50	/	/	/
PBT/AlPi	Original	61.16	28.07	0.83	2.86	/
	Residue	63.01	29.12	2.79	5.08	/
PBT/AlPi/EPM-2	Original	61.50	28.21	0.76	2.62	0.15
	Residue	46.12	34.33	6.04	10.40	3.10

4. Conclusions

An evident improvement in flame retardancy of the PBT composite containing 11 wt% AlPi was achieved by the addition of 0.6 wt% EPM. In terms of UL 94 and LOI measurements, the PBT/AlPi/EPM composite passed V-0 classification with LOI of 37.1%. In contrast to PBT/AlPi, the fire hazard of PBT/AlPi/EPM was suppressed remarkably by a reduction of 16% and 33% in pRSR and TSR. A variation in the flame retardancy mechanism was postulated from the thermal degradation and cone calorimeter results. Small amounts of EPM encouraged the formation of more stable cross-linking char residue and more phosphorus retained in the condensed phase. Solid phase mode dominated the flame retardancy mechanism of the PBT/AlPi/EPM composite.

Acknowledgements

This research work was supported by a grant from Joint Fund of NSFC with Guangdong Provincial Government (U1201243),

National Basic Research Program of China (973 Program, No. 2011CB606002) and the Cultivation Fund of the Key Scientific and Technical Innovation Project, Education Department of Guangdong province (cxzd1008).

Notes and references

- ^a School of Materials Science and Engineering, South China University of Technology, Guangzhou, 510640, P. R. China. Fax & Tel: +86-20-22236818; E-mail: liusm@scut.edu.cn
- ^b The Key Laboratory of Polymer Processing Engineering, Ministry of Education, Guangzhou 510640, P. R. China
- S. V. Levchik and E. D. Weil, *Polym. Advan. Technol.*, 2004, **15**, 691-700.
 - E. D. Weil and S. V. Levchik, *J. Fire. Sci.*, 2004, **22**, 339-350.
 - G. Tang, X. Huang, H. Ding, X. Wang, S. Jiang, K. Zhou, B. Wang, W. Yang and Y. Hu, *RSC. Adv.*, 2014, DOI: 10.1039/C3RA44537B.
 - S. V. Levchik and E. D. Weil, *J. Fire. Sci.*, 2006, **24**, 345-364.
 - S. V. Levchik and E. D. Weil, *Polym. Int.*, 2005, **54**, 11-35.
 - J. Liu, J. Tang, X. Wang and D. Wu, *RSC. Adv.*, 2012, **2**, 5789-5799.
 - U. Braun and B. Scharrel, *Macromol. Chem. Phys.*, 2004, **205**, 2185-2196.

- 8 J. F. Xiao, Y. Hu, L. Yang, Y. B. Cai, L. Song, Z. Y. Chen and W. C. Fan, *Polym. Degrad. Stabil.*, 2006, **91**, 2093-2100.
- 9 P. Liu, M. M. Liu, C. Gao, F. Wang, Y. F. Ding, B. Wen, S. M. Zhang, M. S. Yang, *J. Appl. Polym. Sci.*, 2013, **130**, 1301-1307.
- 5 10 L. Chen, Y. Luo, Z. Hu, G. P. Lin, B. Zhao, Y. Z. Wang, *Polym. Degrad. Stabil.*, 2012, **97**, 158-165.
- 11 S. V. Levchik, D. A. Bright, G. R. Alessio and S. Dashevsky, *Polym. Degrad. Stabil.*, 2002, **77**, 267-272.
- 12 S. Sullalti, M. Colonna, C. Berti, M. Fiorini and S. Karanam, *Polym. Degrad. Stabil.*, 2012, **97**, 566-572.
- 10 13 T. Koppl, S. Brehme, F. Wolff-Fabris, V. Altstadt, B. Schartel and M. Doring, *J. Appl. Polym. Sci.*, 2012, **124**, 9-18.
- 14 S. Brehme, B. Schartel, J. Goebbels, O. Fischer, D. Pospiech, Y. Bykov and M. Doring, *Polym. Degrad. Stabil.*, 2011, **96**, 875-884.
- 15 15 E. Gallo, U. Braun, B. Schartel, P. Russo and D. Acierno, *Polym. Degrad. Stabil.*, 2009, **94**, 1245-1253.
- 16 U. Braun, H. Bahr, H. Sturm and B. Schartel, *Polym. Advan. Technol.*, 2008, **19**, 680-692.
- 17 U. Braun and B. Schartel, *Macromol. Mater. Eng.*, 2008, **293**, 206-217.
- 20 18 S. Hamdani, C. Longuet, D. Perrin, J.-M. Lopez-cuesta and F. Ganachaud, *Polym. Degrad. Stability.*, 2009, **94**, 465-495.
- 19 M. Iji and S. Serizawa, *Polym. Advan. Technol.*, 1998, **9**, 593-600.
- 20 G. M. Wu, B. Schartel, H. Bahr, M. Kleemeier, D. Yu and A. Hartwig, *Combust. Flame.*, 2012, **159**, 3616-3623.
- 25 21 H. Li, Z. Jianqing, S. Liu and Y. Yuan, *RSC Adv.*, 2013, DOI: 10.1039/C3RA45617J.
- 22 Z. T. Wang, X. Zhang, C. Bao, Q. Y. Wang, Y. Qin and X. Y. Tian, *J. Appl. Polym. Sci.*, 2012, **124**, 3487-3493.
- 30 23 N. Didane, S. Giraud, E. Devaux and G. Lemort, *Polym. Degrad. Stabil.*, 2012, **97**, 383-391.
- 24 T. Song, Z. S. Li, J. G. Liu and S. Y. Yang, *Chinese. Chem. Lett.*, 2012, **23**, 793-796.
- 25 A. Vannier, S. Duquesne, S. Bourbigot, A. Castrovinci, G. Camino and R. Delobel, *Polym. Degrad. Stabil.*, 2008, **93**, 818-826.
- 35 26 Z. Wu, S. Li and J. Lu, *J. Wuhan. Inst. Chem. Technol.*, 2006, **1**, 001.
- 27 E. D. Weil, N. G. Patel, M. M. Said, M. M. Hirschler and S. Shakir, *Fire. Mater.*, 1992, **16**, 159-167.
- 28 M. Dzieciol, *Int. J. Environ. An. Ch.*, 2009, **89**, 881-889.
- 40 29 E. Gallo, B. Schartel, U. Braun, P. Russo and D. Acierno, *Polym. Advan. Technol.*, 2011, **22**, 2382-2391.
- 30 A. Factor, *Fire and Polymers*, ACS Publications, Washington, 1990, p. 274.
- 31 G. Socrates, *Infrared and Raman characteristic group frequencies. Tables and Charts*, 3rd ed., John Wiley & Sons, Chichester, 2004.
- 45 32 Y. Qian, P. Wei, P. Jiang, Z. Li, Y. Yan and K. Ji, *Compos. Sci. Technol.*, 2013, **82**, 1-7.
- 33 A. Nodera and T. Kanai, *J. Appl. Polym. Sci.*, 2006, **100**, 565-575.
- 34 B. Schartel and T. R. Hull, *Fire. Mater.*, 2007, **31**, 327-354.